Stochastic noise sources for broadband CAA at geometrical variations of a vehicle

Philipp Uhl[1], Alexander Schell[1], Roland Ewert[2], Jan Delfs[2]

[1]: Aerodynamics and Aeroacoustics Department
Mercedes-Benz AG
Benz-Straße
71063 Sindelfingen

[2]: Institute of Aerodynamics and Flow Technology, Technical Acoustics
German Aerospace Center (DLR)
Lilienthalplatz 7
38108 Braunschweig

Abstract: The Fast Random Particle-Mesh method as member of the class of stochastic noise source methods for broadband aeroacoustic simulations is employed for two test cases and compared to scale-resolving simulations. A side mirror geometry and a full vehicle underbody test case are used to investigate the accuracy and robustness of the method as part of a hydrodynamic-acoustic splitting methodology for nearfield aeroacoustics. The acoustic Deltas of two geometrical configurations of the side mirror are computed with good agreement to reference simulations when choosing a physically agreeing RANS input. Taking minor input data leads to less accurate results. The underbody test case reveals a good performance of the method even for very low frequencies with robustness on three geometrical configurations. With a computational speed-up of a factor of up to 8, the stochastic method proves the capability to be used for broadband noise optimization cycles in very early development stages.

1 Introduction

The automotive industry is rapidly changing due to digital advancements, leading to shorter development cycles and heightened efficiency. A key focus in automotive engineering is reducing noise from aerodynamic sources, called aeroacoustics, which significantly improves passenger comfort. To meet faster development needs, the automotive sector is shifting towards virtual prototyping and simulation-based design. Digital simulations offer cost-effective and efficient ways to evaluate designs and optimize noise reduction before physical prototypes are made, reducing costs and time-to-market. Integrating computational fluid dynamics (CFD) with computational aeroacoustic (CAA) methods provides insights into noise sources and effective mitigation strategies. Advanced computing and numerical methods with e.g. Large

[1] Corresponding author: philipp.uhl@mercedes-benz.com

Eddy Simulations (LES) have transformed aeroacoustic prediction and analysis. However, computational capabilities struggle to match shortened development timelines, highlighting the need for fast yet accurate CAA methods. Stochastic noise source methods based on stationary Reynolds-averaged Navier Stokes (RANS) equations offer promising solutions. These include energy-based methods like Stochastic Noise Generation and Radiation (SNGR) and the correlation-based Fast Random Particle-Mesh (FRPM) method. Both methods realize turbulent velocity fluctuations, with SNGR using random Fourier modes and FRPM utilizing white-noise convolution with predetermined correlations and amplitudes. FRPM has aerospace origins and is yet to be applied in the automotive context.

This paper starts with theoretical remarks on the FRPM method for broadband nearfield aeroacoustics and is followed by two test cases showing the capability of FRPM to deliver consistent and robust noise source data with high accuracy. The last part deals with the computational advantage of the stochastic noise source method.

2 Theoretical remarks

In this section, some theoretical remarks on the used methods are given. The reference simulations are based on two different methods depending on the test case: (i) for the side mirror test case, a Hybrid-Temporal RANS-LES (HTLES) approach as in Duffal et al. [1] with a k-ε Lag Elliptic Blending (LEB) for the sub-filter scales is used, whereas (ii) for the underbody test case, a LES with the WALE sub-gid scale model is chosen. The stochastic noise source method investigated in this work is the Fast Random Particle-Mesh method by Ewert et al. [2] which is explained in the following. A more detailed explanation of the workflow is given in Uhl et al. [3].

2.1 Fast Random Particle-Mesh method

The Fast Random Particle-Mesh (FRPM) method by Ewert et al. [2] used in this work synthesizes stochastic noise sources in the form of turbulent velocity fluctuations in time domain. Time-averaged data from e.g. RANS simulations like the vectorial velocity or scalar turbulent kinetic energy as well as turbulent length scale distribution are necessary as input. With the prescription of frozen turbulence, the method realizes two-point space-time correlations with Gaussian decay in space. The generation of turbulent velocity fluctuations relies on the spatial filtering of a white-noise field $\mathcal{U}_k$ with amplitude $\hat{A}$ with a filter kernel of Gaussian shape G^0:

$$\psi_k(\boldsymbol{x},t) = \int_{V_s} \hat{A}(\boldsymbol{x}) G^0\big(|\boldsymbol{x}-\boldsymbol{x}'|, l_s(\boldsymbol{x}')\big)\mathcal{U}_k(\boldsymbol{x}',t)d\boldsymbol{x}'$$

The curl of the vectorial stream function leads to solenoidal velocity fluctuations $u_i'(\boldsymbol{x},t) = \varepsilon_{ijk}\frac{\partial \psi_k}{\partial x_j}$ since the identity $\nabla \cdot \nabla \times \psi = 0$ holds. The white-noise fields $\mathcal{U}_k$ on the particles introduce the randomness and have zero mean, are mutually

uncorrelated and do not change their value along the streamline for frozen turbulence. The filter kernel G^0 depends on the turbulent length scale distribution l_s which can be derived from RANS via $l_s = c_l \frac{k^{3/2}}{\varepsilon}$ for an ε-based model with $c_l = 0.54$. For an ω-based model, the relation $\varepsilon = C_\mu k\omega$ with $C_\mu = 0.09$ can be used. Turbulence spectra of arbitray shape can be realized, such as Liepmann or von Karman spectra, by superposition of multiple stream functions with different length scale and amplitude. Further details can be found in Wohlbrandt et al. [4].

2.2 Conversion of velocity fluctuations to hydrodynamic pressure fluctuations

The turbulent velocity fluctuations provided by either the scale-resolving simulations like HTLES and LES or the stochastic noise source method FRPM are converted to hydrodynamic pressure fluctuations with the following Poisson equation

$$\frac{1}{\rho}\nabla^2 p_h' = -\frac{\partial^2}{\partial x_i \partial x_j}\left(u_i u_j - \overline{u_i u_j}\right) \quad (\text{with } u_i(\boldsymbol{x},t) = \overline{u}_i(\boldsymbol{x}) + u_i'(\boldsymbol{x},t))$$

which can be derived from the incompressible Navier-Stokes equations. At walls, a Neumann boundary condition $\frac{\partial p_h'}{\partial n} = 0$ and at farfield boundaries with large distance to the source region a Dirichlet boundary condition $p_h' = 0$ is prescribed. This provides a pure hydrodynamic pressure in the nearfield.

2.3 Aeroacoustic analogy

The hydrodynamic pressure field states the driving metric for the acoustic analogy used in this work which is based on a second-order Perturbed Convective Wave Equation (PCWE) derived by Piepiorka and Estorff [5] of the following form

$$\frac{D^2\phi_a}{Dt^2} - c_0^2\nabla^2\phi_a - \frac{1}{\rho}\nabla\phi_a \cdot \nabla p_h' = -\frac{1}{\rho}\frac{Dp_h'}{Dt} \quad \rightarrow \quad p_a' = \rho\frac{D\phi_a}{Dt}$$

which solves for the acoustic potential ϕ_a. The acoustic pressure p_a' is gained by taking the total derivative of the acoustic potential.

3 Side mirror test case

The side mirror is a fundamental noise source in vehicle aeroacoustics and calls a strong attention to itself by being located relatively close to the passenger ears. Due to materialistic coincidence effects of the side window glass, the acoustic pressure p_a' plays the major role for frequencies larger than 1kHz. Therefore, specific experimental studies for validation of numerical methods exist which hold the

hydrodynamic footprint on the side window almost constant with very locally amplifying the acoustic pressure. Such a study is introduced in the following subsection.

3.1 Introduction to test case

In the work of Schell and Cotoni [6], a series side mirror was geometrically modified such that the acoustic footprint on the side window was elevated by approx. 5dB. This was achieved by mounting a forward-facing step with step height of 4mm on the inner, diffusor side of the side mirror. The two geometrical variants can be seen in Figure 1 and are abbreviated with 'plain' and 'step' in the following results.

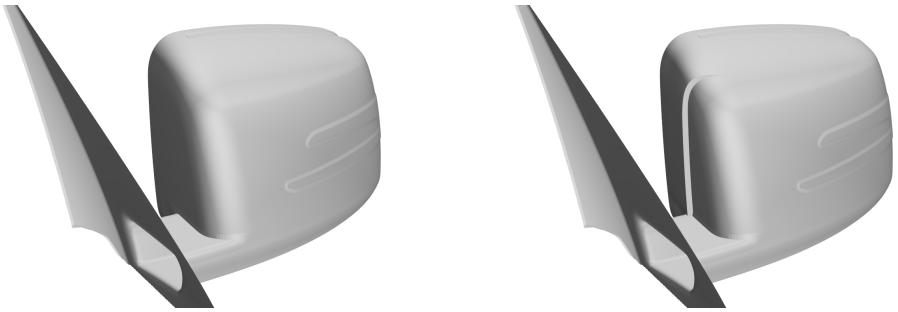

Figure 1: Geometrical variants of the side mirror; left: 'plain' variant, right: 'step' variant with step height 4mm

By experimental wind tunnel tests with artificial heads in the interior of the vehicle as well as beamforming algorithms for acoustic source localization, the acoustic Deltas were proven. Numerical simulations based on the scale-resolving Spalart-Allmaras IDDES approach revealed the acoustic Delta while not changing the hydrodynamic excitation on the side window. The frequency range of interest was 1-5kHz. In this work, the HTLES method with the k-ε LEB model for the sub-filter scales is used. This model delivers identical results to the previously mentioned SA IDDES approach in Schell and Cotoni [6], but is better suited for cross-comparison with FRPM mainly for one reason: FRPM needs two turbulent scales (k and l_s) which are only prescribed by at least a two-equation turbulence model so that for the instationary and stationary computations, a (sub-filtered) turbulence model of the same class is used.

Due to implementation reasons of FRPM, the whole side mirror and side window cannot be included in the source region. Therefore, the source region for FRPM and the HTLES method is only very locally concentrated around the step on the inner side of the mirror with isotropic 1mm cells for FRPM and 0.5mm cells for the HTLES method, see Figure 2. With this small source region, only a little underestimation of 3dB to acoustic results with the whole side mirror are computed showing the high concentration of the acoustic source around the step.

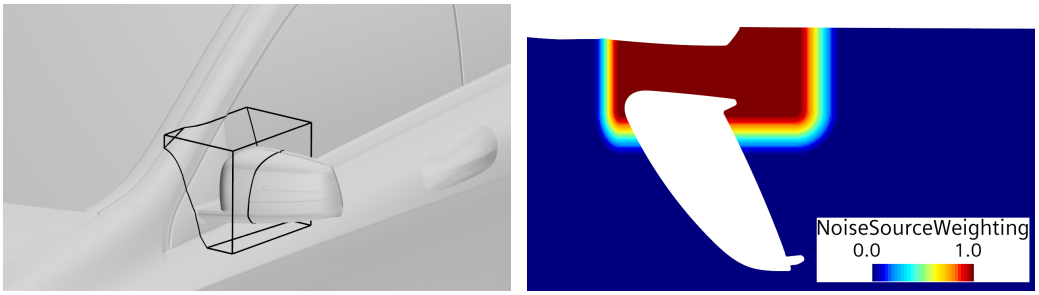

Figure 2: Geometry and source region (left) and noise source weighting function (right) of side mirror test case

3.2 Results of FRPM

This subsection presents broadband noise results by FRPM for both geometrical variants 'plain' and 'step'. The spectra show the integrally averaged power spectral density (PSD) of the acoustic pressure p'_a on the side window. Since the stochastic method does not get along without any empiricism in the form of constants in the turbulent length scale l_s, first the focus is set on the dependence on this parameter by introducing a factor l_{fac} leading to $l'_s = l_{fac} l_s$. This result can be seen in Figure 3 at the geometrical variant with the step.

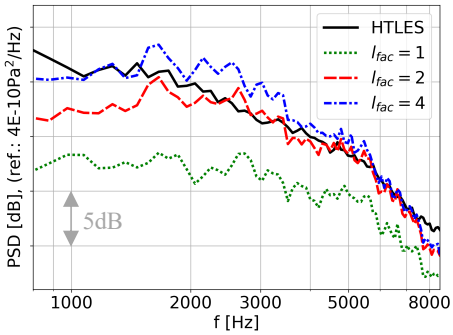

Figure 3: FRPM results of acoustic pressure p'_a on side window based on k-ε LEB for 'step' variant with different l_{fac} compared to HTLES reference simulation

Choosing $l_{fac} = 1$, i.e. using the formula from literature, a massive underprediction is computed. Increasing the turbulent length scale to $l_{fac} = 2$ leads to a very good agreement from $f = 1.5$kHz on. The underprediction for lower frequencies stems from the chosen length scales to be realized by FRPM. In the current configuration, only length scales in 2mm $< l_s <$ 8mm are computed by means of 5 Gaussians leading to a Liepmann spectrum. The reason for the better agreement with higher l_{fac} is that by increasing the length scale, the step is taken more into account since the length scales from RANS are then shifted in the length scale interval and the realized turbulent kinetic energy focusses more around the step. The FRPM spectra are in very good agreement up to 7kHz from where on a faster decay compared to the HTLES

method occurs. This can either have its reason in less numerical noise or in the grid size which amounts uniformly 1mm compared to 0.5mm in the volume mesh of the HTLES method. Increasing the length scale even more ($l_{fac} = 4$) leads to a slight overprediction in a mid-frequency range from 1.5-5kHz.

Choosing $l_{fac} = 2$ as default settings due to the agreement of absolute levels also for the 'plain' mirror variant results in the integrally averaged spectra on the side window in the left part of Figure 4.

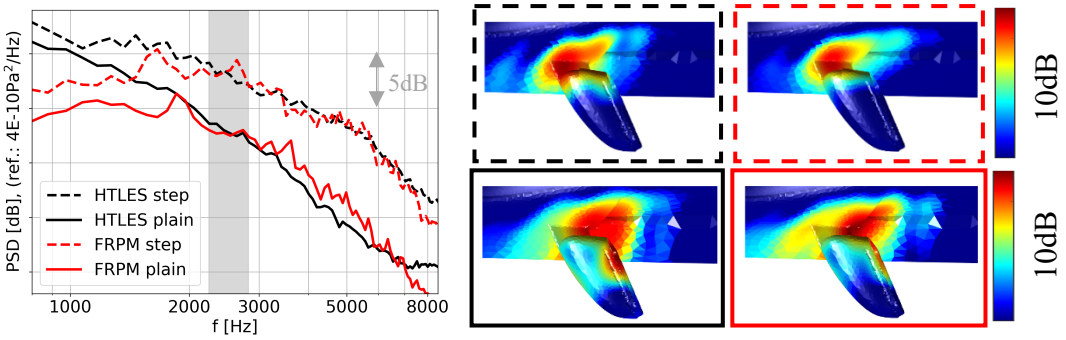

Figure 4: FRPM results of p'_a on side window with $l_{fac} = 2$ based on k-ε LEB for both geometrical variants (left) and beamforming results for third-octave band with center frequency $f_c = 2.5$kHz (right); colorbars with 10dB dynamic each apply rowwise (+7dB for the 'step' variant)

As can be seen, a good agreement for 1.5-7kHz can be achieved. The low-frequency underestimation can be traced back to the missing, larger length scales. Including these improves the agreement for $f < 1.5$kHz but introduces high-frequency noise from 5kHz on. These results are not shown here. Remarkable is the high-frequency behavior from the FRPM fluctuations as the decay is very uniformly whereas the HTLES method has a slight amount of numerical noise indicated by the stagnation in the spectra. This underlines the solenoidal and clean realization of turbulent velocity fluctuations by FRPM. In the gray area in Figure 4, the third-octave frequency band with center frequency $f_c = 2.5$kHz is shown. In this frequency band, a beamforming algorithm is applied with sampling of the acoustic pressure in a plane with top view on the side mirror. Experimental data in Schell and Cotoni [6] showed an upstream shift of the acoustic source from the trailing edge for the 'plain' variant to approx. the position the step with the 'step' variant. This can be reproduced by both approaches, HTLES and FRPM, shown in the right half of Figure 4 and verifies the high-quality stochastic sources of FRPM.

To further investigate the robustness of FRPM on the input data, the acoustic Deltas are also shown when starting with $l_{fac} = 1$, i.e. with an FRPM configuration that underpredicts the absolute levels. This can be seen in Figure 5 by visually comparing the shaded areas between the two FRPM variants to the HTLES spectra. The FRPM variants are artificially shifted downwards as indicated in the legend entries.

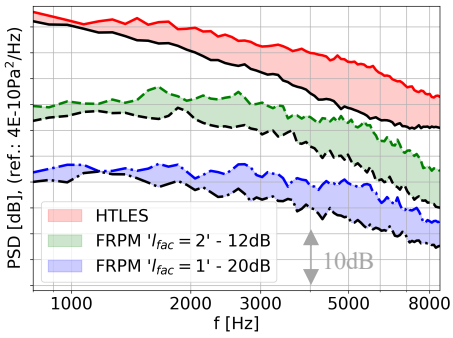

Figure 5: FRPM results of p'_a on side window for both geometrical variants with $l_{fac} = 2$ and $l_{fac} = 1$ compared to reference HTLES

The spectra show the robustness of FRPM to react on geometrical variations. This performance is a fundamental key to the usage for optimization purposes since relative changes in the flow phenomena should lead to relative differences in the acoustic radiation even though the absolute agreement could not be given since a scale-resolving reference simulation may not exist.

The last open question to be answered is the performance of FRPM based on a RANS model that is not of the accuracy as the k-ε LEB. Therefore, the k-ε Realizable (Real.) is chosen. The derivation of the turbulent length scale is identical for both models. To be in touch with absolute HTLES results, the k-ε Real. is calibrated with $l_{fac} = 2.2$. This leads to Figure 6 with acoustic Deltas on the left and with some insights into the flow phenomena on the right:

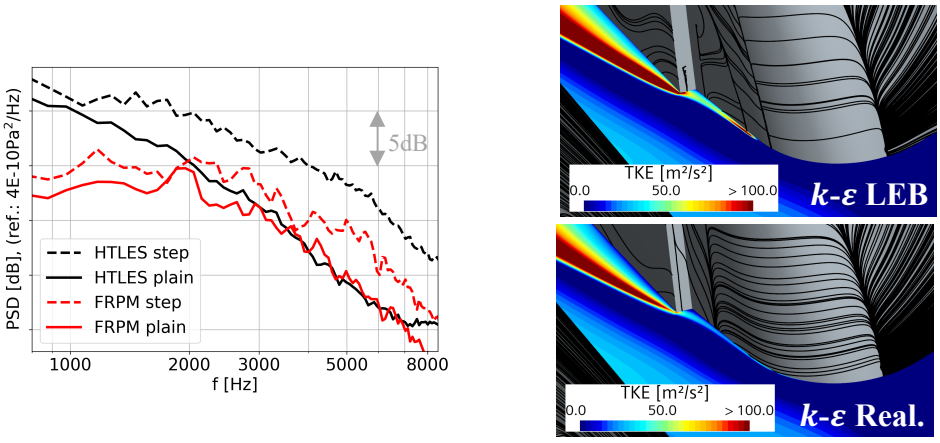

Figure 6: FRPM results of p'_a on side window based on k-ε Real. (left) and flow phenomena (right) with turbulent kinetic energy (TKE) and surface streamlines

Whereas the 'plain' variant might have an acceptable agreement to the reference simulation, the 'step' variant is massively underpredicted. This can be traced back to the flow phenomena. The k-ε LEB computes a separation bubble on the inner side near the leading edge of the mirror with some high production of the turbulent kinetic energy close to the bubble. The k-ε Real. starts with a turbulent boundary layer and does not exhibit this behavior. Although the separation bubble is acoustically not

relevant, and in FRPM due to the grid size not represented, it provides higher TKE values for downstream interaction with the step leading to higher acoustic amplifications close to this source region. This turbulence model study reveals the necessity for good input data to expect acoustic results with good agreement to high-fidelity simulations.

4 Underbody test case

In a next step, the focus is set on low frequencies in a range from 50-800Hz. This frequency range is mainly excited by the underbody flow between the car and the ground which can be best investigated with a very simplified yet realistic geometry.

4.1 Introduction to test case

The AeroSUV is a simplified car geometry developed by Zhang et al. [7] which has different geometrical variants in the underbody flow, the degree of detail of the underbody structure as well as engine bay flows. In a first step, the engine bay is closed and the variant with flat underbody is chosen. The source region is taken around the right front wheel due to symmetry effects of the vehicle. A visual representation of the test case and the size of the source region is given in Figure 7:

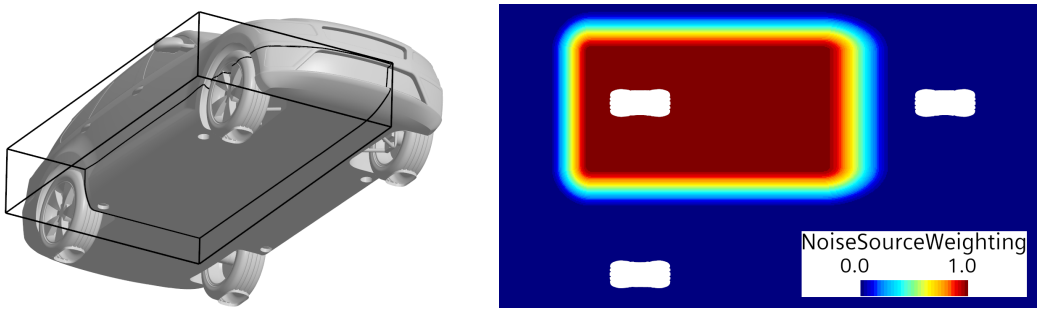

Figure 7: Geometry and source region (left) and noise source weighting function (right) of AeroSUV test case

The original investigation of the AeroSUV does not cover any aeroacoustic results and was performed in a model wind tunnel with a 1:4-scaled model geometry. Therefore, in this work, the geometry is scaled up by a factor of 4 to enable realistic frequency values.

4.2 Results of FRPM

It is especially emphasized here that the given results in this subsection on the AeroSUV are ongoing work. The results show promising agreement with scale-resolving simulations; however the open question will be answered in future works

why approaches like FRPM with isotropy in the Reynolds stresses as well as in the length scales are suitable for such kind of problems. The results shown in Figure 8 are achieved on an isotropic Δx=8mm grid.

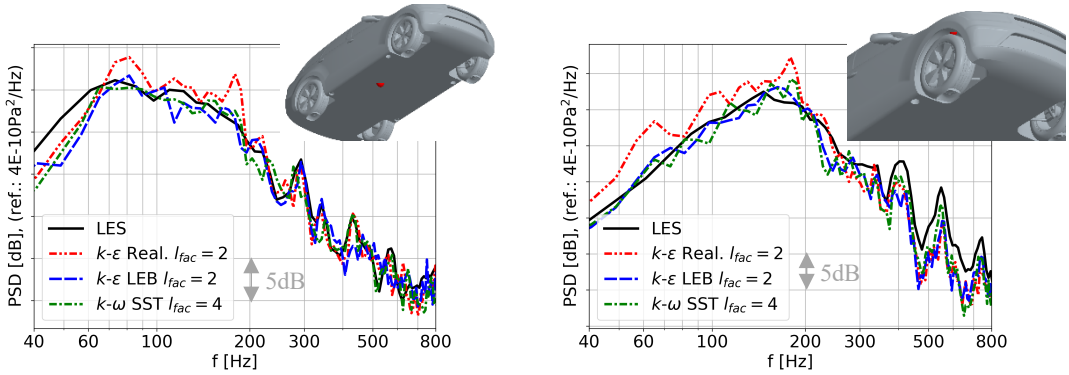

Figure 8: Point spectra of p'_a for three different turbulence model inputs; points indicated with red dots; left: on underbody, right: in wheelhouse

Two different points are shown for the variant with the flat underbody – in the wake of the right front wheel inside the noise source region and in the top part of the wheelhouse covered mostly by the wheel outside the noise source region. Therefore, three RANS models are used: the k-ε Real., the k-ε LEB as well as the k-ω SST model. Both points show a very promising agreement over the whole frequency range of interest from 40 to 800Hz. The peaks in the spectrum indicating modes by geometric features are also captured. A further validity of the FRPM approach to deliver accurate source data for CAA can be seen in Figure 9 showing streamlines colored with the root-mean-square (RMS) of the acoustic source $-1/\rho\ Dp'_h/Dt$. The streamlines are generated on the (mean) velocity vector for the reference LES (left) and the k-ε LEB variant (right).

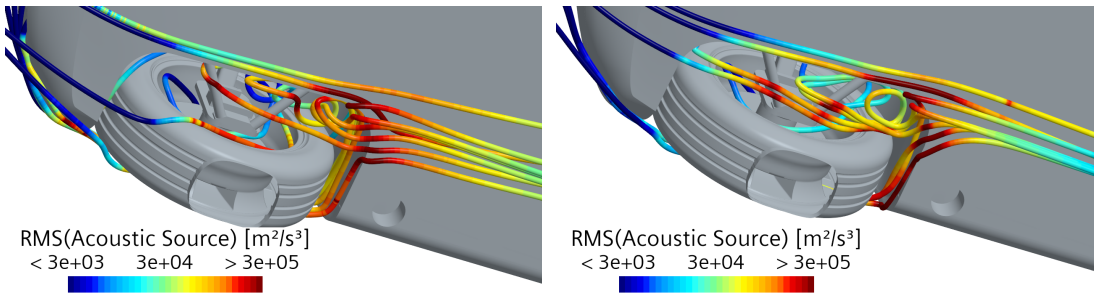

Figure 9: Root-mean-square of acoustic source for PCWE for LES (left) and FRPM based on RANS k-ε LEB (right)

A conglomeration of high acoustic source values in the close wake of the wheel colliding with the downstream located edge of the flat underbody can be observed for both simulations. This region is not coinciding with the region of maximum turbulent kinetic energy which is far downstream of the front wheels at the downstream end of the source region.

Further investigating the Delta prediction capabilities of FRPM leads to slightly differing geometries for the flat underbody configuration shown in Figure 10. As a first simplification to the default (black frame), the wheels are closed with planar surfaces to prevent a flowthrough (red frame). In a second step, the wheelhouse is completely closed to remove this resonance volume and the downstream edge of the underbody at which high acoustic source values are observed (blue frame):

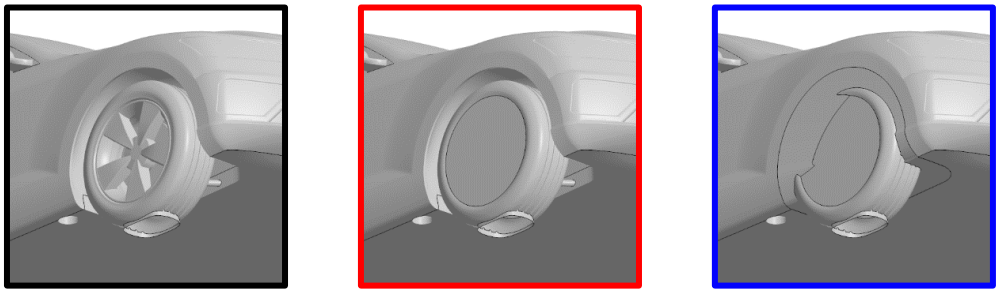

Figure 10: Geometrical modifications on front wheels (red) and wheelhouses (blue compared to default variant (black)

The results in the acoustic pressure for a point in the centerline at approximately the x-position of the wheel is given in Figure 11.

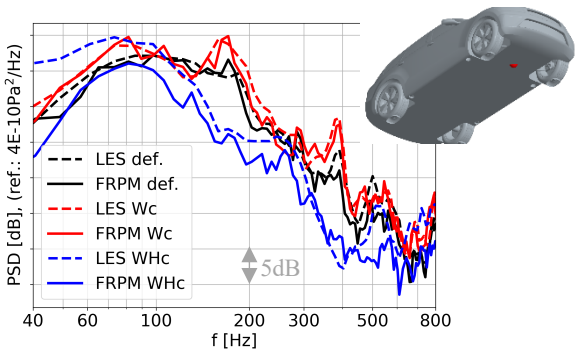

Figure 11: Point spectra of p'_a for LES (dashed) and FRPM (solid) for three variants (see Figure 10); legend: *Wc* = wheels closed, *WHc* = wheelhouse closed

FRPM reacts correctly on both geometrical modifications. The slight elevation of the levels with the closed wheels compared to the open wheels in the default configuration especially at 180Hz and 380Hz is in very good agreement. For the entirely closed wheelhouses on the front axle, the trend is also computed although FRPM reacts a bit too strong by underestimating the overall levels slightly at mid frequencies of 100-300Hz and with stronger disagreement for lower than 100Hz and between 500Hz and 600Hz. However, the overall trend is captured.

As an outlook for future work regarding the underbody acoustics of the AeroSUV, more detailed and hence realistic underbody geometries are taken. These are also available in the package of geometry data provided for this vehicle test case.

5 Computational effort of methods

In this section, a short comparison of the computational efforts of the different methods is given with the CPU hours normalized to the reference simulation of each test case. The reference workflow consists of the stationary initialization with a RANS and the transient reference initialization followed by final reference CAA simulation. The stochastic workflow is based on the same RANS as the reference simulation but continues with the realization of fluctuations with the FRPM method with storing on the hard drive and ends with the CAA simulation induced by those FRPM fluctuations by importing from the hard drive.

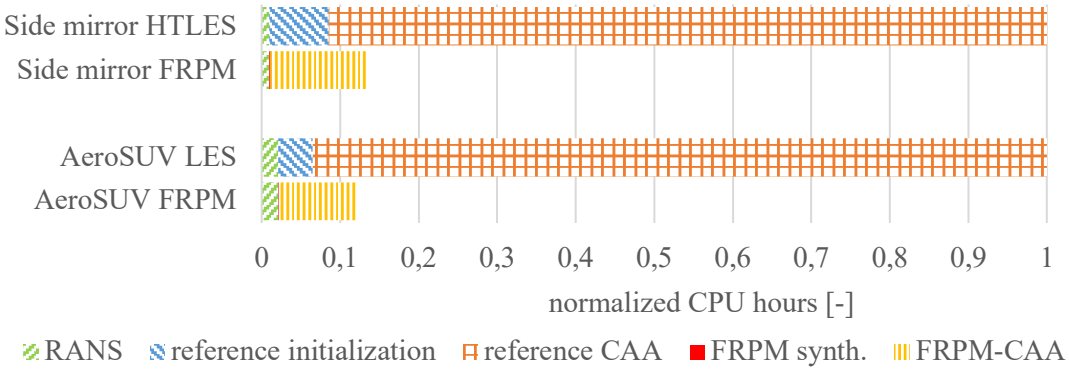

As one can see, for both test cases a similar picture is drawn in terms of computational advantage with a speed-up of approximately a factor of 8. The bottleneck in the simulation process so far is the import of the velocity fluctuations from the hard drive in the FRPM-CAA step. Removing this step with an on-the-fly implementation in one simulation environment is expected to lead to an additional speed-up of a factor of 2-3 in the FRPM-CAA step.

6 Conclusion and outlook

Stochastic noise source methods like the Fast Random Particle-Mesh method can be a significant enabler for optimization regarding broadband noise in the field of computational aeroacoustics. Therefore, several conditions need to be fulfilled: (i) accuracy of the results, (ii) robustness and (iii) consistency of the method. Accurate in the sense of only minor deteriorated results compared to existing scale-resolving reference simulation, robust by predicting trends of modified input data similarly to reference simulations (e.g. geometrical modifications) and consistent in the sense of the quality of input data (e.g. usage of different turbulence models). These three points are worked out in a different degree of detail for two test cases: a high-frequency side mirror test case and a low-frequency underbody test case by means of a Hydrodynamic-Acoustic Splitting approach based on a Poisson equation and a second order Perturbed Convective Wave Equation. For the side mirror test case, very accurate results for two different geometries of the mirror are achieved compared to a high-resolved Hybrid-Temporal RANS-LES approach. With a RANS simulation

capturing the important flow aspects, a good agreement is achieved whereas using a RANS without these phenomena leads to only partially good agreement. The underbody test case is still ongoing work but shows very promising results with less sensitivity on the used turbulence model. Geometrical variants are investigated with overall good agreement in the acoustics. The benefit of stochastic noise source methods with enhanced modelling assumptions comes across with an enormous computational speed-up of a factor of approx. 8.

7 References

[1] V. Duffal, B. de Laage de Meux and R. Manceau, "Development and Validation of a Hybrid RANS-LES Approach Based on Temporal Filtering," in *Proceedings of the ASME-JSME-KSME 2019 8th Joint Fluids Engineering Conference*, San Francisco, California, USA, 2019.

[2] R. Ewert, J. Dierke, J. Siebert, A. Neifeld, C. Appel, M. Siefert and O. Kornow, "CAA broadband noise prediction for aeroacoustic design," *Journal of Sound and Vibration,* vol. 330, no. 17, pp. 4139-4160, 2011.

[3] P. Uhl, A. Schell, R. Ewert and J. Delfs, "Validation of the Fast Random Particle-Mesh Method for Broadband CAA of a Forward-Facing Step and its prediction sensitivity for geometrical modifications," in *AIAA AVIATION 2023 Forum*, San Diego, California, USA, 2023.

[4] A. Wohlbrandt, N. Hu, S. Guérin and R. Ewert, "Analytical reconstruction of isotropic turbulence spectra based on the Gaussian transform," *Computers & Fluids,* vol. 132, pp. 46-50, 2016.

[5] J. Piepiorka and O. von Estorff, "Numerical investigation of hydrodynamic / acoustic splitting methods in finite volumes including rotating domains," in *23. International Congress on Acoustics*, Aachen, Germany, 2019.

[6] A. Schell and V. Cotoni, "Flow Induced Interior Noise Prediction of a Passenger Car," *SAE International Journal of Passenger Cars - Mechanical Systems,* vol. 9, 2016.

[7] C. Zhang, M. Tanneberger, T. Kuthada, F. Wittmeier, J. Wiedemann and J. Nies, "Introduction of the AeroSUV - A New Generic SUV Model for Aerodynamic Research," in *WCX SAE World Congress*, Detroit, Michigan, USA, 2019.